Boundary-Layer Meteorol (2009) 131:223–243
DOI 10.1007/s10546-009-9368-4

ARTICLE

Influence of Thermal Effects on the Wind Field Within the Urban Environment

R. Dimitrova · Jean-François Sini · K. Richards · M. Schatzmann · M. Weeks · E. Perez García · C. Borrego

Received: 23 January 2008 / Accepted: 24 February 2009 / Published online: 11 March 2009

Abstract Micrometeorological conditions in the vicinity of urban buildings strongly influence the requirements that are imposed on building heating and cooling. The goal of the present study, carried out within the Advance Tools for Rational Energy Use towards Sustainability (ATREUS) European research network, is the evaluation of the wind field around buildings with walls heated by solar radiation. Two computational fluid dynamics (CFD) codes were validated against extensive wind-tunnel observations to assess the influence of thermal effects on model performance. The code selected from this validation was used to simulate the wind and temperature fields for a summer day in a specific region of the city of Lisbon. For this study, the meteorological data produced by a non-hydrostatic mesoscale atmospheric model (MM5) were used as boundary conditions for a CFD code, which was further applied to analyze the effects of local roughness elements and thermodynamic conditions on the air flow around buildings. The CFD modelling can also provide the inflow parameters for a Heating, Ventilation and Air Conditioning (HVAC) system, used to evaluate the building energy budgets and to predict performance of the air-conditioning system. The main finding of the present three-dimensional analyses is that thermal forcing associated with the heating of buildings can significantly modify local properties of the air flow.

Keywords Code validation · Computational fluid dynamics · Microscale meteorological models · Thermal effects

R. Dimitrova · J.-F. Sini (✉)
Laboratoire de Mécanique des Fluides, Ecole Centrale de Nantes,
1, rue de la Noë, BP 92101, 44321 Nantes Cedex 3, France
e-mail: Jean-Francois.Sini@ec-nantes.fr

K. Richards · M. Schatzmann
Meteorological Institute, University of Hamburg, Hamburg, Germany

M. Weeks · E. Perez García · C. Borrego
Department of Environment and Planning, University of Aveiro, Aveiro, Portugal

R. Dimitrova
Center for Environmental Fluid Dynamics, Arizona State University, Tempe, AZ, USA

1 Introduction

The influence of air flow around buildings and the effects of urban heating on local micro-climate (i.e. the urban heat island effect) have been addressed in numerous studies, with a limited number focussed on the thermal effects related to the wall heating on the flow regime in close proximity to buildings (Nakamura and Oke 1988; Oke 1988; Ruck 1993; Mestayer et al. 1995; Sini et al. 1996; Kim and Baik 1999, 2001; Santamouris et al. 1999; Uehara et al. 2000; Louka et al. 2001; Kovar-Panskus et al. 2002a,b; Huizhi et al. 2003; Bohnenstengel et al. 2004; Xie et al. 2007). The numerical results obtained until now remain predominantly inconsistent with field and laboratory experiments, which investigated the influence of thermal wall effects on the flow pattern around buildings.

Numerical studies of solar radiation effects on the modification of classical isothermal flow within street canyons show that the flow pattern primarily depends on the wind speed at the roof-top level, the exposure of the heating wall(s), and the canyon aspect ratio H/W, where W is the street canyon mean width and H is the characteristic height of buildings. Previous studies were mainly focused on two-dimensional flows under a wide variety of street canyon aspect ratios, covering different types of flow regimes: skimming flow, wake interference flow and isolated roughness flow (Oke 1988). For canyons with an aspect ratio $H/W \approx 0.5$, the disturbed air flow has insufficient distance to readjust before encountering the downwind building, resulting in wake interference flow. In the case of regular canyons ($H/W \approx 1$), the bulk of the large-scale flow glides over the street producing a skimming flow, which is characterised by the formation of a single vortex within the canyon (Hunter et al. 1992). In the skimming flow regime, which appears in relatively deep street canyons ($H/W > 1$), the transition from a one-vortex to a two-vortex regime, and from a two-vortex to a three-vortex regime, occurs as the aspect ratio increases. Different street canyon aspect ratios that influence the flow, together with the heated walls, depend on the wind direction, i.e. leeward or windward. The impact of the vortices inside the canyon depends on the wind speed at the roof-top level, but their shape and strength can be affected by thermal effects induced by differential heating of the walls and/or the bottom of the canyon (Mestayer et al. 1995; Sini et al. 1996; Kim and Baik 1999, 2001; Louka et al. 2001; Xie et al. 2007). It has been shown that the thermally-induced air flow in close proximity to a heated vertical surface either strengthens or weakens a mechanically forced flow, producing a single vortex ($H/W = 1$) or two counter-rotating vortices ($H/W = 2$). Note that in deeper canyons ($H/W > 3$) the flow modification is more complex. In this case, the horizontal flow speed at the ground level is too low and therefore thermally-driven upward motion splits the lowest vortex in the flow forming two adjacent counter-rotating vortices (Kovar-Panskus et al. 2002a; Xie et al. 2007). Other studies show that increases of the wall-air temperature difference produces, in some cases, additional vortices. These results are related to the ground level or windward wall heating (Mestayer et al. 1995; Sini et al. 1996; Kim and Baik 1999, 2001), and clearly suggest that the cross-canyon vortex structure is influenced by canyon heating, which depends on the heating wall exposure, the canyon ratio, and the difference between the wall and ambient temperatures.

Validations of most numerical studies against laboratory and field data are limited. Kim and Baik (2001) used the wind-tunnel observations of Uehara et al. (2000) to validate model performance only for a limited combination of parameters, such as $H/W = 1$ and temperature difference $\Delta T = 2°\mathrm{C}$. The predictions of the normalised potential temperature and horizontal velocity profiles were in fair agreement with the observed flow structure and its modification due to the thermal effects. However, the model was not tested for various heating

configurations, while the thermal flow predictions of Mestayer et al. (1995), Sini et al. (1996) and Kim and Baik (1999) also remain untested.

Wind-tunnel experiments also showed further inconsistency with numerical predictions; the experiments of Kovar-Panskus et al. (2002b) and Huizhi et al. (2003) are the only experimental studies directly related to the wall heating thermal effects on the flow dynamics within street canyons, though they are not directly comparable. Kovar-Panskus et al. (2002b) conducted measurements in a wind tunnel using a two-dimensional square-section canyon model, applying heating to a windward wall. Huizhi et al. (2003) used a water tank with ground-heated flow in non-symmetrical urban street canyons, and found that under near-zero ambient wind the flows in the street canyon are completely driven by thermal effects. Horizontal and vertical motions were also generated above the buildings roofs. In a two-dimensional cavity with $H/W = 1$, Kovar-Panskus et al. (2002a) observed a cross-canyon circulation with no significant alterations of the flow structure generated by the windward wall heating (the initial conditions were $U = 0.5$–$1\,\mathrm{m\,s^{-1}}$, temperature difference $\Delta T \approx 50°\mathrm{C}$, which equates to $\Delta T \approx 5°\mathrm{C}$ for a full-scale case with $H = 20\,\mathrm{m}$). While the equivalent full-scale ΔT is comparable to that used in the windward wall heating numerical experiments, the modified flow structure appeared to be clearly inconsistent with the laboratory results of Kovar-Panskus et al. (2002b).

In a combined numerical and field study, Louka showed that the CHENSI numerical model [that used by Mestayer et al. (1995) and Sini et al. (1996)] overestimated thermal effects of the windward wall heating, predicting two counter-rotating vortices when only one recirculation vortex was observed during the field experiment ($H/W = 1.4$, $\Delta T = 18°\mathrm{C}$). The quantification of thermal effects on the airflow dynamics close to the wall (within 1.5 m) was incomplete because of a lack of velocity measurements at the locations of the temperature sensors and traffic effects. During the field measurements in a 14.85-m wide canyon, a sharp horizontal temperature difference ($\Delta T = 10.7°\mathrm{C}$) was observed within 20 mm of the building wall; the temperature difference remained high (2.9°C) within the next 0.2 m, but then fell sharply as distance from the wall increased. These observations implied the presence of a very thin thermal wall boundary layer.

As was already stated, numerical models overestimate the influence of wall-heating thermal effects and predict significant changes in flow regime compared to the experimental studies. This disagreement with experimental data is believed to be due to inaccurate representation of the near-wall thermal conditions in numerical models. The standard wall function (Sini et al. 1996) has been validated for a thick thermal boundary layer (Lévi Alvares 1991) and is widely used in different CFD models. The atmospheric (Louka et al. 2001) and wind-tunnel (Richards et al. 2006) observations showed, however, a very thin thermal boundary layer, which required a modification to the wall function. The standard wall function provides a good shape for the temperature profile, but overestimates the magnitude close to the heated wall (Dimitrova et al. 2007).

In the present study, within the scope of the ATREUS Project, two CFD numerical models (microscale models) were tested against observations from the controlled wind-tunnel experiments of Richards et al. (2006). The experimental data helped to optimize the effect of a thin thermal boundary layer in numerical models and further demonstrate the ability of CFD codes to simulate three-dimensional flow and improve results of the Heating, Ventilation and Air Conditioning (HVAC) system ENER-WIN (Degelman Engineering Group Inc., 2005: http://members.cox.net/enerwin), providing more detailed inflow conditions.

2 Wind-Tunnel Experiment

The wind-tunnel experiments were designed to validate CFD microscale numerical models, with a single building with leeward wall heating (Fig. 1) used. This simplification is essential for understanding the influence of heating by solar radiation on the flow dynamics around an obstacle and with careful consideration of the conditions described above, a 1:100 scale model of a single building (a cube) was designed.

The cube was placed in a multi-layered wind tunnel where the upstream flow was generated using a large number of a sharp-edge roughness elements, and upstream vortex generators were used to produce a turbulent boundary layer. The inflow profile for the subsequent numerical simulations was measured at a distance of four cube heights ($4H$) upstream.

An important governing parameter in this flow is the Richardson number Ri, and in thermal convection studies the Richardson number can be presented as a combination of the Grashof (Gr) and Reynolds (Re) numbers, which are the ratios of buoyancy and viscous forces, and inertial and viscous forces, respectively. Here

$$Ri = \frac{Gr}{Re^2} = \frac{\beta g H(\overline{T}_w - \overline{T}_{ref})}{\overline{U}_{ref}^2}, \tag{1}$$

where β is the of thermal expansion coefficient, g is the acceleration due to gravity, H is the building height, $\overline{T}_w$ is the mean wall temperature, $\overline{T}_{ref}$ is the upstream ambient temperature, and $\overline{U}_{ref}$ is the reference wind speed upstream of the model domain. When $Gr/Re^2 \approx 1$, the flow is controlled by both thermal and mechanical effects; for $Gr/Re^2 >> 1$, the buoyancy effects dominate the flow formation.

The experiments were performed for flow parameters representative of a combination of free and forced convection (the mixed case, $Gr/Re^2 \approx 1.6$ and 0.9) and for a pure forced convection $\left(Gr/Re^2 \approx 0.1\right)$ and low wind speed conditions were employed in order to maximise thermal effects. The mean flow speed around the cube was measured using a two-dimensional fibre-optic laser Doppler anemometer with $0.05\,\mathrm{m\,s^{-1}}$ accuracy. The mean (3-min averaging) longitudinal, lateral and vertical velocity components were recorded along with their root-mean-square values, while Reynolds shear stresses were calculated for the same time intervals. The mean temperature was measured using E-type thermocouples. A series of experiments were conducted, including measurements of the velocity field around

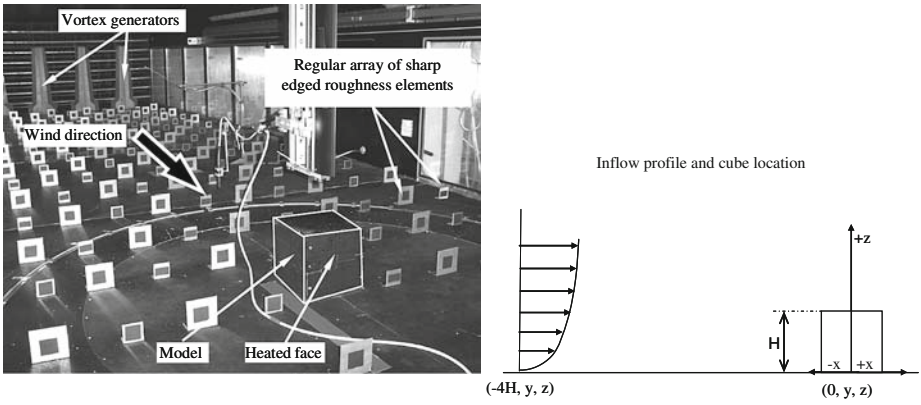

Fig. 1 The experimental set-up in the wind tunnel

the non-heated cube and measurements of the mean temperature and velocity in the wake of the cube under different thermal conditions. The experimental details and main results can be found in Richards et al. (2006).

3 Model Validation

CHENSI (Sini et al. 1996) and VADIS (Martins and Borrego 1998) CFD research codes were used in this study, both employing the steady-state Reynolds-averaged Navier-Stokes (RANS) equations for the balance of momentum and mass conservation, with the Boussinesq eddy-viscosity approximation and the k-ε turbulence closure to calculate the mean and turbulence flow patterns around the cube.

CHENSI was developed in the Laboratory of Fluids Mechanics at Ecole Centrale de Nantes, France, and solves the governing equations for three-dimensional flows and a transport equation for the mean concentration of a passive pollutant. A finite volume method is applied on a non-uniform staggered grid. The Reynolds stress, the heat fluxes and the concentration fluxes were estimated using the Boussinesq eddy-viscosity and eddy-diffusivity schemes. The popular two-equation k-ε model (Jones and Launder 1972), which refers to the balance of turbulent kinetic energy (TKE) and its dissipation rate, was implemented; the commonly accepted values for empirical modelling constants used for industrial flows (Launder and Spalding 1974) were assigned. A mediocre performance of this model is often attributed to the modelling of the dissipation rate equation and progress is usually achieved by modifying this equation. Chen and Kim (1987) suggested adding an additional time scale to the dissipation equation, which enables more effective energy transport from large-scale to small-scale components of the flow. This extra term, along with an additional modelling constant, was added to the standard k-ε model implemented in CHENSI. A comparison of the results using both turbulent models showed that the modified scheme gives a better prediction specifically in the impingement region (Dimitrova et al. 2007). The described CFD code was used to simulate air flow and traffic pollutant dispersion at microscales, as well as to analyse the thermal effects of solar radiation on the airflow (Kim and Baik 1999, 2001; Louka et al. 2001; Kovar-Panskus et al. 2002b). CHENSI has been employed also in several intercomparison studies (Ketzel et al. 2001; Sahm et al. 2002; Vardoulakis et al. 2006).

VADIS was developed at the Department of Environment and Planning, University of Aveiro, Portugal as a tool to estimate the dispersion of pollutants in the atmosphere, and consists of two modules FLOW (CFD model) and DISPER (Lagrangian dispersion model). FLOW uses a numerical solution of the three-dimensional RANS equations and the k-ε turbulence closure to calculate wind, turbulent viscosity, pressure, and temperature fields. VADIS has a capacity to support a multi-obstacle and multi-source environment, as well as non-stationary flows and emissions. The evaluation of maximum short-term local concentrations for urban geometries, especially under low wind speed conditions, can be simulated (Martins and Borrego 1998). The simulation results were validated using wind- tunnel measurements (Borrego et al. 2000). More recently VADIS has been applied to the Lisbon downtown area, demonstrating good performance for the flow patterns and dispersion around obstacles under variable wind conditions (Borrego et al. 2003, 2004, 2007). VADIS also has been used in previous model intercomparison studies (Sahm et al. 2002; Vardoulakis et al. 2006).

CHENSI and VADIS were tested for a non-uniform inlet flow and thermal coupling against wind-tunnel observations discussed by Richards et al. (2006), to assess these codes for predicting wind and temperature fields around a three-dimensional obstacle.

3.1 Computational Domain

The size of our computational domain exactly matched the dimensions of the laboratory experiment, which was 2.1 m × 1.6 m × 1.1 m (see Fig. 2). A uniform grid with a resolution of 0.0095 m (20 times less than the cube size $H = 0.19$ m) was chosen for VADIS and a non-uniform stretched grid with the highest resolution of 0.0095 m close to the walls was used for CHENSI.

3.2 Isothermal Case: Results and Discussion

Non-uniform inflow fields were used for the calculations to account for the flow inhomogeneity observed in the laboratory experiment. A linear space interpolation was applied between the available experimental data for velocity (u) and turbulent kinetic energy (k) at the location $x/H = -4$, where the upstream vertical boundary profiles were measured at three different horizontal levels: $y/H = -1.5$, 0.0, and 1.5.

Several statistical metrics were calculated to quantify the performance of both models against the experimental data, viz.
the normalized mean bias:

$$NMB = \frac{\sum_{i=1}^{N} (P_i - O_i)}{\sum_{i=1}^{N} O_i}, \tag{2a}$$

the normalized mean error:

$$NME = \frac{\sum_{i=1}^{N} |P_i - O_i|}{\sum_{i=1}^{N} O_i}, \tag{2b}$$

where P is the predicted value, and O is the observed value.

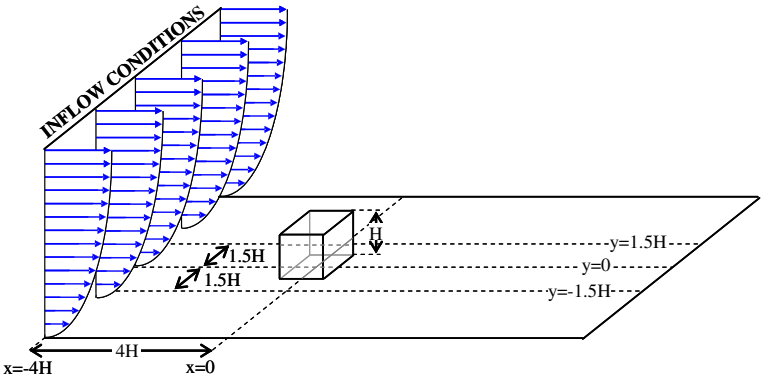

Fig. 2 A sketch of the computational domain

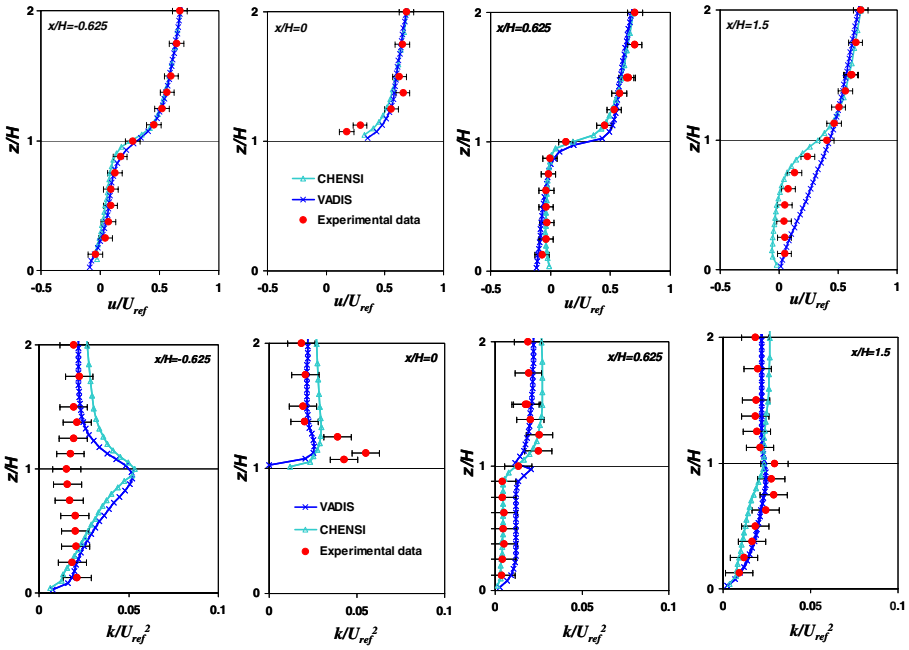

Fig. 3 The observed and calculated vertical profiles of the non-dimensional longitudinal velocity component and turbulent kinetic energy at different locations in the cube centre plane

The comparisons of the vertical profiles of the u component and the energy k were taken at different locations, which are shown in Fig. 3 for various distances x/H from the cube centre. The agreement between numerical and experimental results is reasonable for the longitudinal velocity, except downstream of the cube, where VADIS simulates the reattachment point closer to the obstacle, while CHENSI predicts a more distant position of this point (the reattachment point x_S is the point where flow impinges on the surface and separates in opposite directions along the wall). At the location $x/H = 1.5$, CHENSI tends to produce a negative u near the ground ($NMB = -0.21$), while VADIS computes a positive u ($NMB = 0.25$), indicating a different size of the predicted recirculation vortex. Both models overestimate the turbulent kinetic energy (NMB is about 0.7) in the impingement region $x/H = -0.625$ and fail to predict strong vertical shear at the top of the obstacle $x/H = 0$ ($NMB = 0.09$ for CHENSI and -0.27 for VADIS). VADIS simulates the TKE in better agreement with the experimental data near the re-attachment point $x/H = 1.5$ compared to CHENSI ($NMB = 0.004$ and -0.12 respectively), but CHENSI gives a better prediction close to the leeward cube side within the cavity zone $x/H = 0.625$ ($NMB = 0.64$ for CHENSI and 0.32 for VADIS).

The horizontal distributions of the normalized u and TKE values are shown in Fig. 4 at $z/H = 0.5$ for the impingement region $x/H = -0.625$, the cube centre $x/H = 0$ and near the experimentally obtained reattachment point $x/H = 1.5$. The models reproduce well the horizontal velocity field observed in the wind tunnel upstream and around the obstacle, with NMB in the range -0.09 to 0.12. The main difference appears downstream of the cube, beyond $x/H = 1.5$. CHENSI underestimates the longitudinal velocity component ($NMB = -0.27$) while VADIS gives better agreement with the measured values ($NMB = 0.09$). There is a discrepancy between the calculated and observed values of turbulent kinetic energy, where

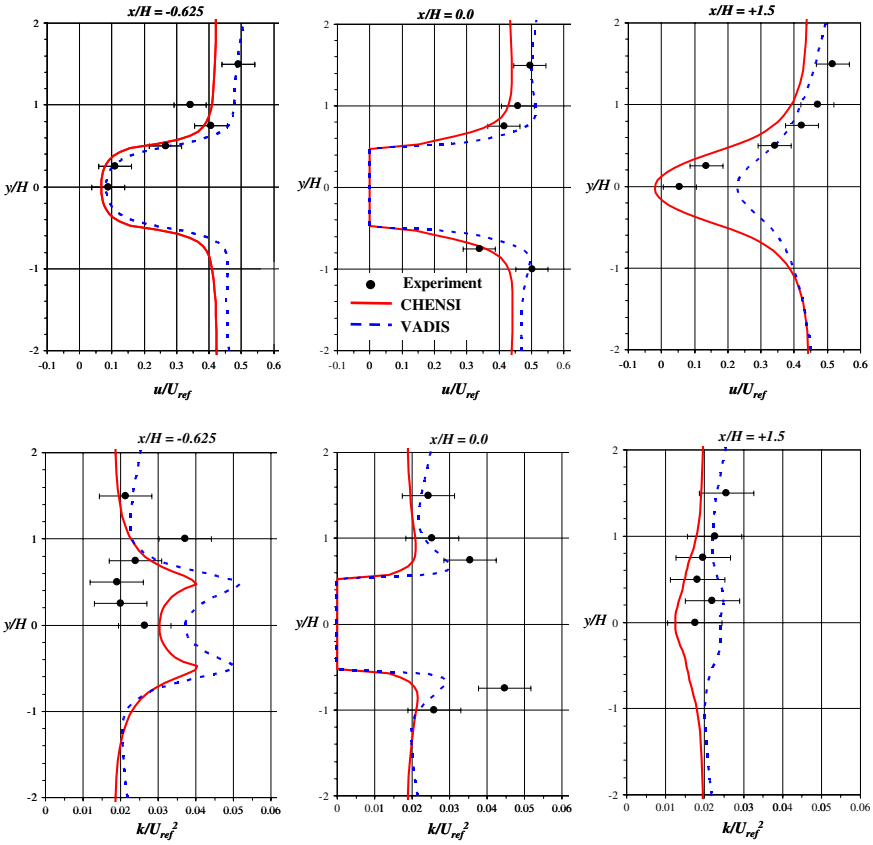

Fig. 4 Horizontal distributions of the non-dimensional velocity and turbulent kinetic energy at $z/H = 0.5$

the peak values predicted by the models are at the line of the cube lateral edges. In the impingement area $x/H = -0.625$ the observed maxima, however, are shifted away from the obstacle ($NMB = 0.17$ for CHENSI and 0.4 for VADIS). Both models fail to predict the observed values of TKE very close to the obstacle at $x/H = 0$. The calculated turbulent kinetic energy again significantly differs from the observations downstream of the cube, at $x/H = 1.5$, with VADIS overestimating ($NMB = 0.12$), and CHENSI underestimating ($NMB = -0.25$) the measured values.

The mean normalized errors and bias calculated for the vertical profiles (Table 1) and horizontal distributions (Table 2) of the u velocity component and turbulent kinetic energy k are presented at different locations corresponding to the same locations as those shown in Figs. 3 and 4. The largest discrepancies between the calculated and measured velocity profiles for both models was found close to the re-attachment point $x/H = 1.5$, while a large disagreement for k is shifted to the impingement region $x/H = -0.625$. Both models produced largest errors in the horizontal distributions of u downstream of the cube, while for the turbulent kinetic energy, the biggest disagreement with the experimental data is located upstream of the obstacle.

Table 3 summarizes important characteristics of the flow around the obstacle predicted by CHENSI and VADIS codes and those obtained in the laboratory measurements. Both models

Table 1 The mean normalized and fractional errors of the calculated velocity and turbulent kinetic energy vertical profiles at different non-dimensional locations x/H (see Fig. 3)

x/H	u velocity component				Turbulent kinetic energy k			
	NME		*NMB*		*NME*		*NMB*	
	CHENSI	VADIS	CHENSI	VADIS	CHENSI	VADIS	CHENSI	VADIS
−0.625	0.125	0.068	−0.119	−0.037	0.819	0.755	0.743	0.730
0.0	0.156	0.171	0.021	0.071	0.441	0.358	−0.088	−0.271
0.625	0.125	0.068	−0.119	−0.037	0.188	0.544	0.064	0.316
1.5	0.213	0.297	−0.205	0.252	0.289	0.144	−0.116	0.004

Table 2 The mean normalized and fractional errors of the calculated u velocity component and turbulent kinetic energy horizontal distributions at different non-dimensional locations *x/H* (see Fig. 4)

x/H	u velocity component				Turbulent kinetic energy k			
	NME		*NMB*		*NME*		*NMB*	
	CHENSI	VADIS	CHENSI	VADIS	CHENSI	VADIS	CHENSI	VADIS
−0.625	0.165	0.133	−0.087	0.116	0.386	0.589	0.166	0.399
0.0	0.105	0.124	−0.089	0.116	0.340	0.201	−0.340	−0.201
1.5	0.274	0.227	−0.274	0.087	0.250	0.161	−0.250	0.116

Table 3 Characteristic scales of the flow

Characteristic scales	CHENSI	VADIS	EXPERIMENT
Stagnation point z_S/H	0.8	0.8	0.7
Reattachment length x_R/H	1.89	1.23	1.34
Separation length x_S/H	−0.77	−0.53	−0.75

predicted a higher value for the height of the stagnation point z_S (where the upcoming flow approaches the windward side of the obstacle and separates); CHENSI overestimated the re-attachment length x_R while VADIS underestimated it; CHENSI made a better estimate of the upwind vortex length (x_S) than VADIS.

3.3 Thermal Case: Results and Discussion

Different values of the governing parameter Gr/Re^2 were selected in order to assess the influence of thermal effects on the flow patterns. The simulations were performed for $Gr/Re^2 \approx 0.9$ and $Gr/Re^2 \approx 1.6$, corresponding to the experiments described above (see Sect. 2). Figure 5 shows the non-dimensional temperature profiles (T/T_{ref}) observed in the wind tunnel and those predicted by CHENSI and VADIS at the cube central plane for $Gr/Re^2 \approx 1.6$. The simulated temperature profiles are significantly different especially close to the heated wall. VADIS overestimates temperature near the heated cube face ($x/H = 0.55$), but modelling results are closer to the measurements in the wake of the cube ($x/H = 0.625$). A tendency for amplification of buoyancy effects can be seen in the vertical temperature profiles produced by VADIS; a disagreement with the experimental data is also found downstream above the

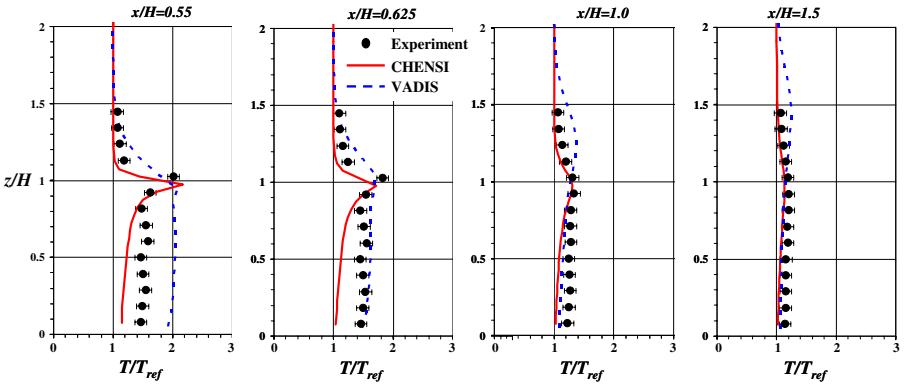

Fig. 5 Vertical profiles of non-dimensional temperature (T/T_{ref}) at the cube centre plane at different downstream locations for $Gr/Re^2 \approx 1.6$

Table 4 The mean normalized and fractional errors of the calculated temperature at different non-dimensional locations x/H for $Gr/Re^2 \approx 1.6$ (see Fig. 5)

x/H	*NME*		*NMB*	
	CHENSI	VADIS	CHENSI	VADIS
0.55	0.115	0.283	−0.071	0.264
0.625	0.195	0.082	−0.195	0.066
1.0	0.104	0.110	−0.104	−0.007
1.5	0.073	0.071	−0.073	−0.012

cube height. The normalized mean and fractional errors, calculated for both models against experimental data, are shown in Table 4. The errors are less than 0.2, except for VADIS results in close proximity to the heated wall, where the errors are up to 0.28.

Figure 6 compares experimentally and numerically obtained contour plots of T/T_{ref} at the cube centre plane, with the velocity vectors superimposed for strong thermal conditions. A thermal plume that results from the air heating close to the cube surface is clearly detectable in the experimental data. As this warmer, less dense, air interacts with the cooler mechanically driven flow from the top of the cube it is washed downstream, producing the elongated temperature distribution at the upper trailing edge of the cube, where the maximum temperatures are observed. The result implies that the heated air is mainly transported vertically to the top of the cube and then advected horizontally by the thermal plume, with no re-entrainment into the wake through the recirculation region. The temperature field predicted by CHENSI shows disagreement with the experimental data mainly within the cavity zone close to the ground; this significant difference seems to be associated with strong upward flow within a vertical circulation induced by the heated cube face. The spatial temperature distribution produced by VADIS shows the over-production of buoyancy, as the warmer air plume is raised over the top of the cube, which disagrees with the experimental results. The heated air flows downstream from the leeward cube face mainly above the cube height, $z/H = 1$, and a strong upward flow, produced by the air heating near the cube face, is directed towards the top (and above) of the leeward side. We see that higher temperatures are observed in the recirculation bubble close to the ground ($T/T_{ref} \approx 1.25$ at $x/H = 1$), and probably due

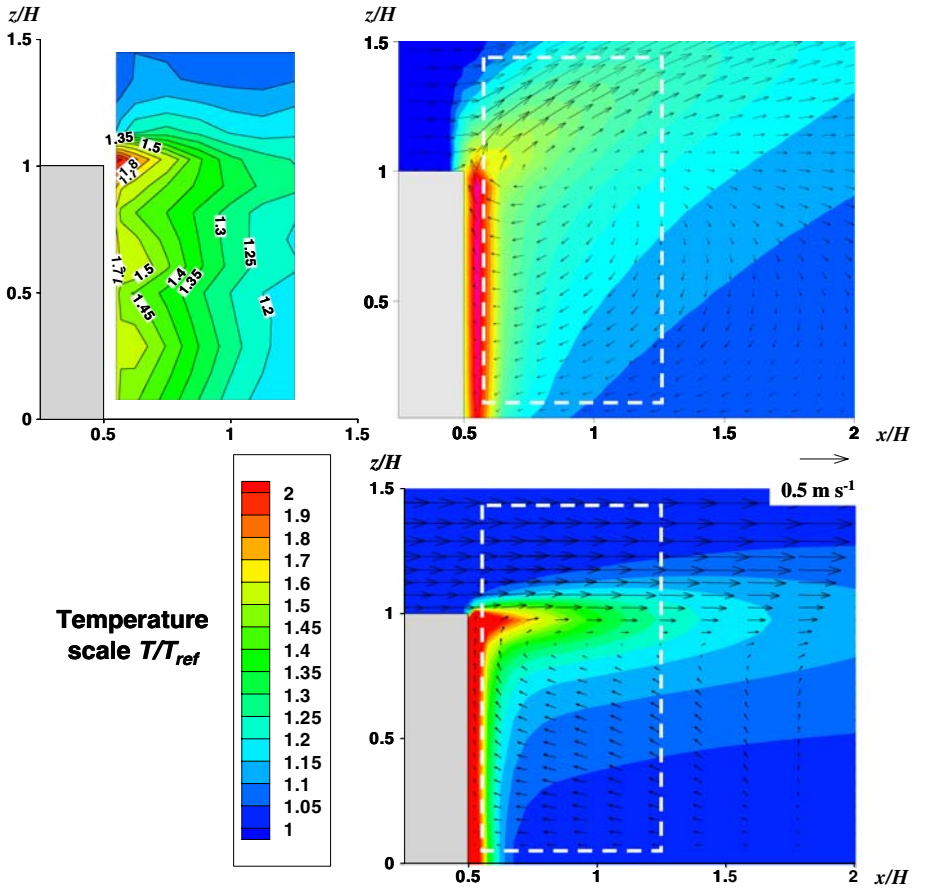

Fig. 6 The non-dimensional temperature and velocity fields at the cube centre plane $y/H = 0.0$ for $Gr/Re^2 \approx 1.6$

more to heat conduction from the cube to the ground than to heat convection in the wake. This effect was not taken into account in the numerical simulations.

Figure 7 shows the horizontal structure of the temperature field obtained experimentally and numerically at the non-dimensional height $z/H = 0.7$, where CHENSI predicts a very similar temperature pattern that was observed in the wind tunnel. The maximum temperatures appear near the lateral cube faces, although this numerical model overestimates the temperature close to the heated cube face. This may be associated with the conduction heat losses at the boundary in the laboratory experiment. For numerical simulations, a uniform initial temperature distribution was prescribed, although this was not, however, the exact case in the experimental set-up, where a constant heat flux produced a non-uniform temperature distribution due to heat loss close to the cube face boundary and heat conduction in the ground. The differences in simulated and measured temperatures can be found far from the heated cube face along the cube centre plane due to high horizontal velocity of the calculated reversed flow. VADIS predicted a more uniform temperature distribution in the horizontal plane and failed to produce the temperature maxima close to the lateral cube boundaries.

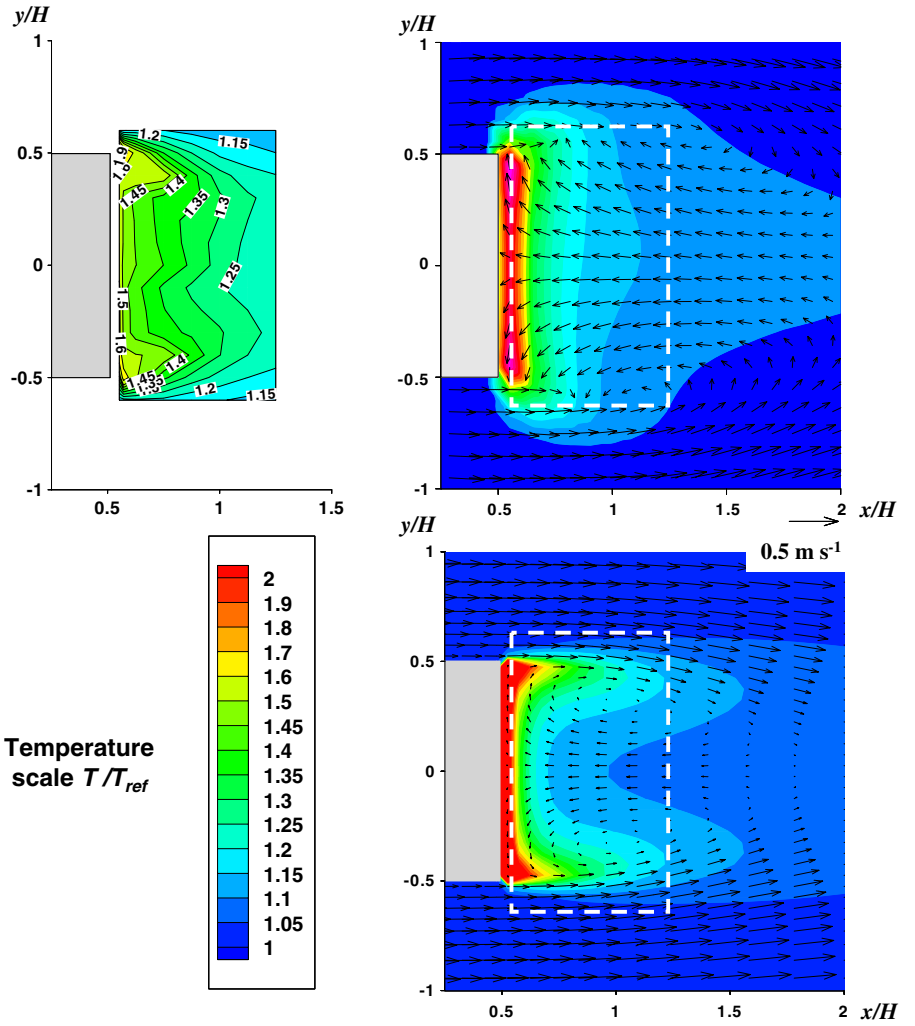

Fig. 7 The non-dimensioned temperature and velocity fields for $Gr/Re^2 \approx 1.6$ at the vertical level $z/H = 0.7$

3.4 Section Summary

Both models utilized the same RANS equations, with a uniform grid used for VADIS simulations and a non-uniform grid with the same mesh size close to the walls employed by CHENSI. CHENSI exploited a modified k-ε model, while VADIS implements the standard scheme. This can produce the difference in the flow patterns obtained by both models for the isothermal case. The modification of the turbulent model reduces disagreement with experimental data, specifically in the impingement region, where the standard k-ε model tends to overproduce turbulent kinetic energy.

Overall differences between the VADIS and CHENSI simulations for the thermal case were fairly significant. A large amount of heat is advected to the cube top creating noticeable differences between the two models for the temperature field. The main reason for this

discrepancy is that VADIS used the standard wall functions, which led to a higher temperature close to the heated cube face producing a stronger buoyancy force at the top of the cube. The CHENSI performance was in better agreement with the wind-tunnel temperature field due to the modified wall function, having lower mean normalized bias and errors compared to VADIS. Because of this, we only used CHENSI for further calculations in the Lisbon street canyon.

4 CFD Modelling of the Thermal Effects: "Lisbon Case"

The CFD code CHENSI was used to predict the flow field (including the thermal effects of solar heating) within a complex array of buildings with modelling geometry based on an urban block in the city of Lisbon, Portugal.

4.1 Modelling Approach

The computational domain included a group of 26 obstacles with a simplified uniform building height of 15 m, and a domain orientation 16° east of north. A stretched grid (with the highest space resolution of 2 m close to the obstacles) was used for the street canyon modelling (Fig. 8), and a two-building configuration (the lower panel of Fig. 8) within the computational domain was used further for the building modelling. The profiles produced by CHENSI at point A (see the lower panel of Fig. 8) were used as the input conditions for the HVAC simulation model (these results are not included in this study).

4.2 Input and Boundary Conditions

The mean wind velocity, turbulent kinetic energy and temperature profiles were produced by the non-hydrostatic mesoscale model MM5 (http://www.mmm.ucar.edu/mm5) at a coarse resolution (1 km × 1 km) grid (Fig. 9). The profiles served as input conditions for the CHENSI model so as to simulate the airflow dynamics in Lisbon for a typical summer day (July 9, 2000) at 0100, 0800, 1500, and 2200 local time; an extreme thermal condition was used at 1400 local time. The terms "typical day" and "extreme thermal conditions" are based on preliminary statistics over long time series of meteorological data for the Lisbon region (Oxizidis et al. 2008); a "typical day" refers to the most frequently occurring circulation and diurnal temperature variations in July. The classification system, developed by H. Lamb, was used to classify the weather types on a daily basis (Kelly et al. 1997). The "extreme thermal conditions" refer to strong solar radiation [the daily global radiation is approximately 28,000 kJ m^{-2} $(24\,h)^{-1}$], which leads to a maximum energy consumption for the air conditioning of buildings.

Upscaling was used to specify the temperature distribution at the walls. The boundary conditions were obtained by HVAC with the inflow conditions generated by MM5, and the temperature at the boundaries of selected buildings nested within the computational domain was calculated for a typical street canyon aspect ratio $H/W = 1$ (the domain is shown in the lower panel of Fig. 8) depending on the sun exposure. A sketch showing the consecutive steps of our modelling approach and the corresponding feedbacks is given in Fig. 10.

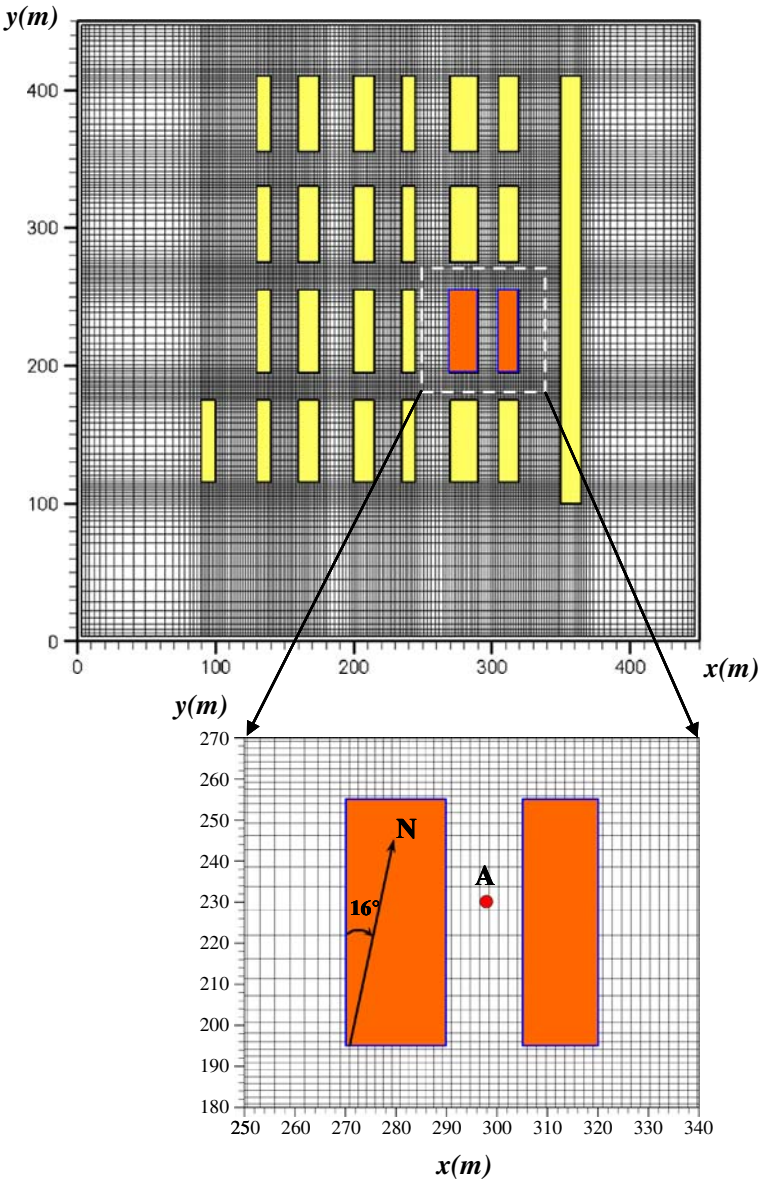

Fig. 8 The computational grid used for microscale numerical simulations

4.3 Results and Discussion

The inflow profiles of the velocity components, turbulent kinetic energy, and temperature are shown in Fig. 11 and the CFD simulated profiles are presented in Fig. 12. The inflow velocity (Fig. 11) did not change significantly during most of the day, except at 2200 local time. Relatively strong uniform winds ($u \approx 10\,\mathrm{m\,s^{-1}}$, direction ≈340–350°) characterized the overall meteorological conditions. The CDF profiles (Fig. 12) signify the flow properties

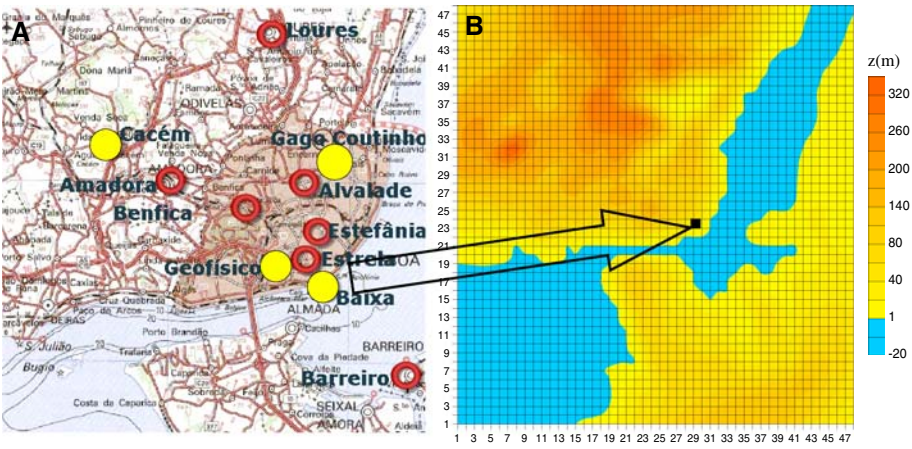

Fig. 9 Lisbon domain and computational grid used for the mesoscale numerical simulations

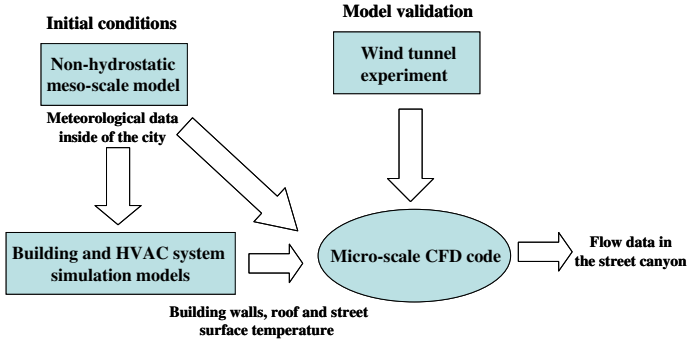

Fig. 10 Methodological parameters used in the study

at the centre of a narrow street canyon between two selected buildings (point A in Fig. 8), and will be further used as the new inflow conditions for the HVAC model to account for the microscale urban effects.

The CFD horizontal velocity component declined within the street canyon cavity contrary to the vertical velocity, which showed a maximum at the building roofs. The TKE decreased within the cavity zone with its maximum predicted by CHENSI at approximately two building heights. In contrast, the MM5 vertical profiles show a steady increase of TKE upwards. The temperature profiles within the street canyon simulated by CHENSI show an increase of temperature during the hours of high solar radiation (1400–1500 local time) in contrast to the uniform MM5 temperature profiles. A local temperature maximum within the canyon cavity and a strong vertical gradient near the building roofs can be seen in Fig. 12 (specifically at 1400, 1500, and 2200 local time). The vertical profiles predicted by CHENSI, compared to the MM5 results, show a significant influence of thermal building effects leading to the increase of flow inhomogeneity, due to direct solar heating of the street canyon during the day or its cooling at night. Because of the reduced turbulence and lower wind speeds within the street canyon cavity with regard to the inflow profiles, different wall heating significantly increased the temperature within the street canyon, particularly at 1400 and 1500 local time, when the

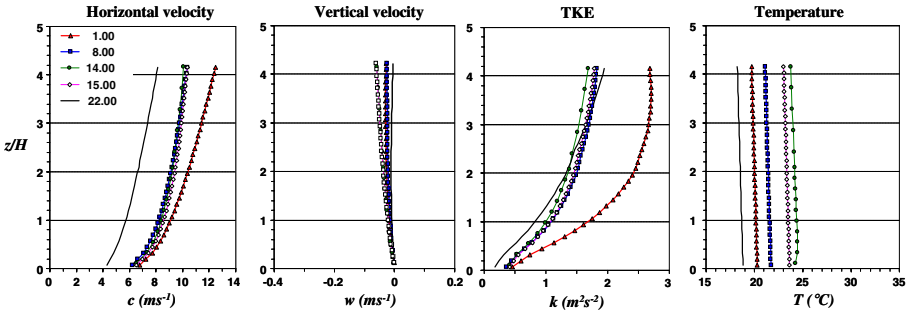

Fig. 11 Inflow profiles produced by the non-hydrostatic mesoscale model MM5 at different times of the day

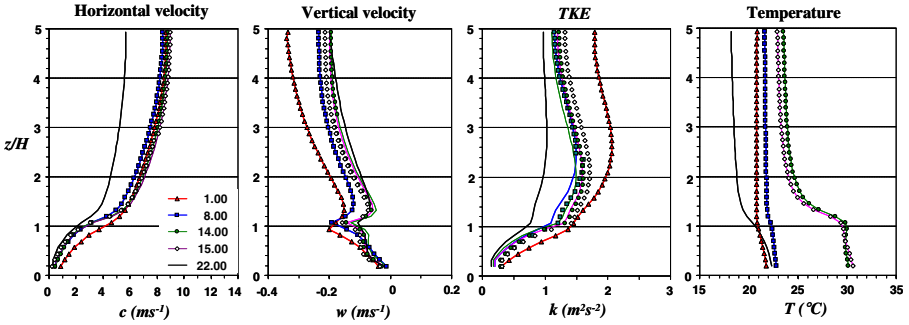

Fig. 12 The velocity components, TKE, and temperature profiles simulated by the CFD model accounting for local urban effects at the different times of the day

temperature difference between the heated surface (≈40°C) and ambient air (≈24°C) was large.

A comparison between the isothermal case (without building heating) and the thermal case at 1500 local time (with the same inflow conditions) demonstrates strong thermal influence on flow dynamics. The results are presented in Figs. 13 and 14 for the street canyon with the aspect ratio $H/W = 1$, where the velocity vectors and contours are shown. A difference between the isothermal and thermal cases is found for the vertical and horizontal velocity components, when the vector of the reference velocity is not parallel to the street axis (section A). A weak flow modification was observed for a nearly parallel reference flow (section B). Both A and B cross-sections show one dominant vortex within the canyon, and for the almost perpendicular reference flow (section A), the vortex centre is shifted to the top of the building (see arrow in Fig. 14-A). A strong temperature gradient was generated between the building surface and the ambient air. The dynamic and buoyancy factors act in opposite directions and therefore the intensity of the single vortex decreases in comparison to the isothermal flow. The heated air close to the windward building face upwells and interacts with the dynamically-induced downward flow, which leads to a net decrease of the vertical velocity magnitude (from 0.5 to 0.2 m s^{-1}). The wall heating can largely influence the intensity of the vertical flow.

The modelling results for the street canyons with different aspect ratios (between regular canyons $H/W = 1$ and the avenue canyons $H/W \approx 0.5$) are shown for different flow characteristics at 1500 local time in Figs. 15, 16 (velocity components), 17 (TKE), and 18 (the temperature difference between local and reference values). A clear distinction should be

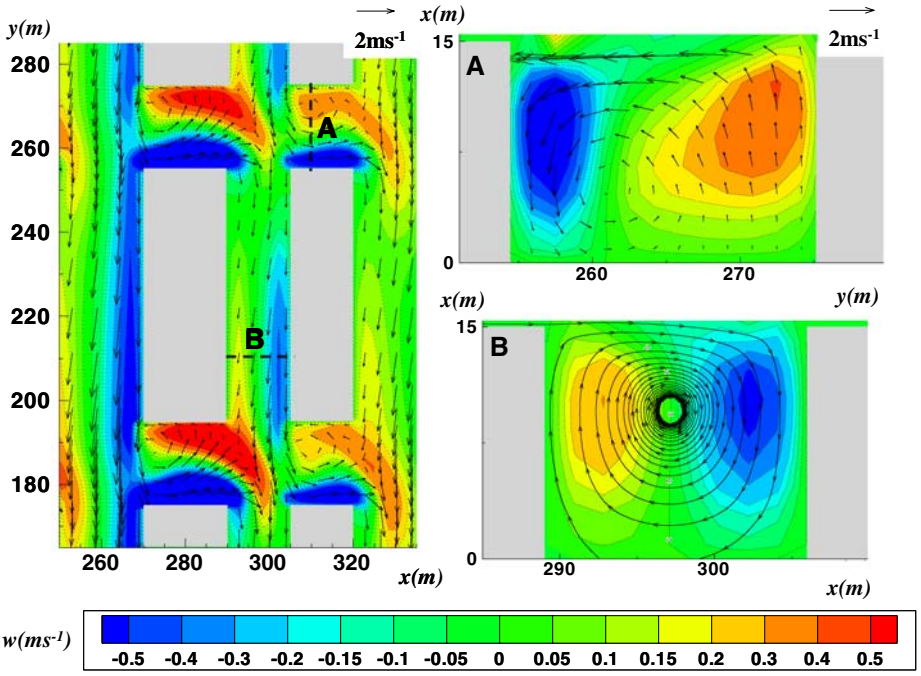

Fig. 13 Vertical velocity field and corresponding vectors/streamlines at 1500 local time; the isothermal case

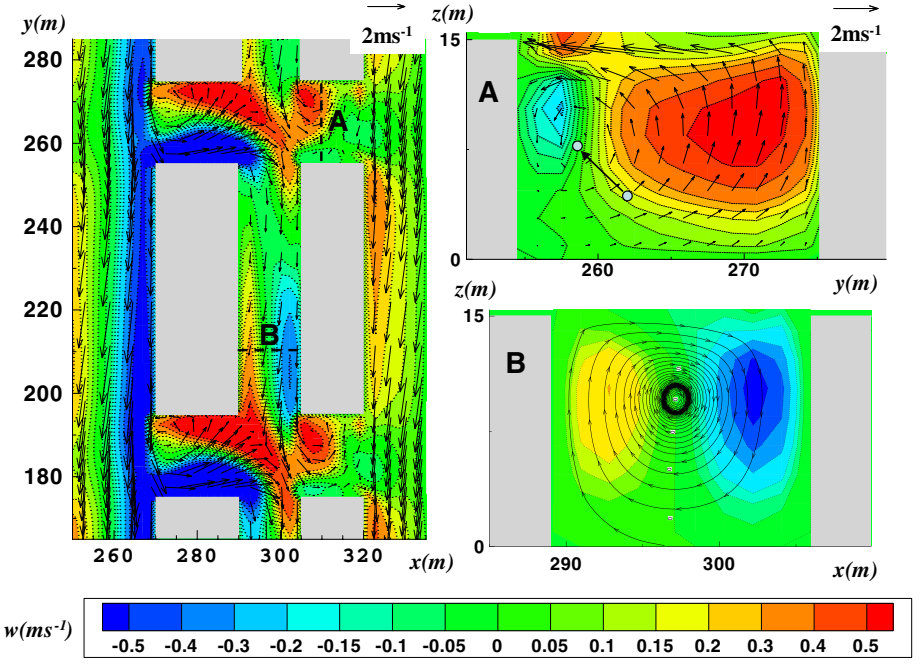

Fig. 14 Vertical velocity field and corresponding vectors/streamlines at 1500 local time; the thermal case

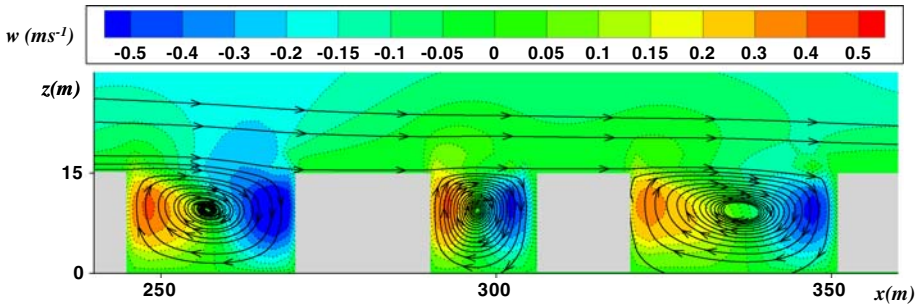

Fig. 15 Vertical velocity field and streamlines (u and w components) for different aspect ratios $H/W = 0.6$, 1.0, and 0.5 at 1500 local time

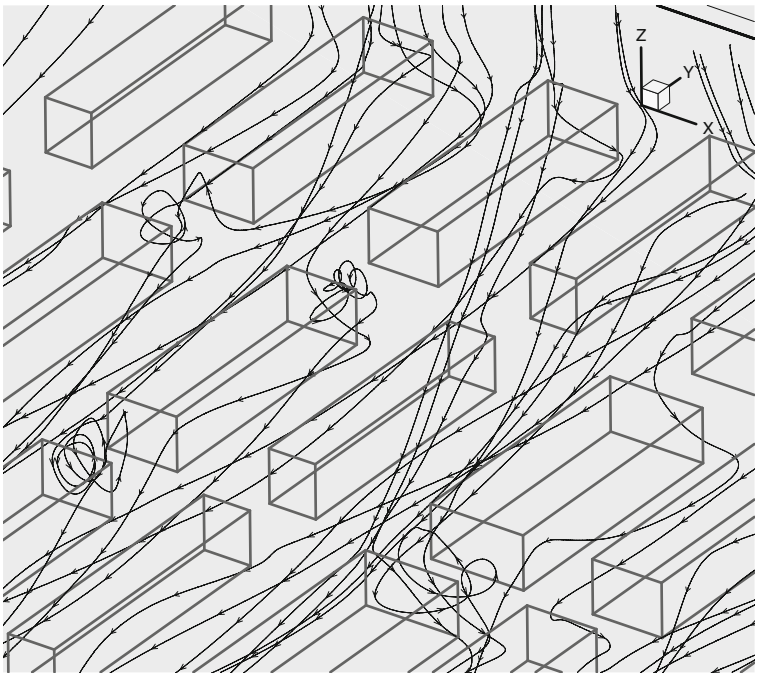

Fig. 16 The three-dimensional streamlines (u, v, and w components) at 1500 local time

made between the synoptic wind conditions above the roof-top level and local winds within the cavity of the canyon. A near-parallel synoptic airflow with strong winds (approximately $8\,\mathrm{ms}^{-1}$) was simulated by MM5 for this case. All three-dimensional flows considered in our calculations for different aspect ratios are characterized by a single clockwise rotating vortex (Fig. 15), which is formed due to the deflection of the airflow from the windward wall of the canyon. For oblique roof-level winds this deflection may induce a spiral wind flow through the canyon, while other complex channelling effects could be produced by winds parallel to the street axis. A complex influence of the above mentioned factors on the street canyon wind flow is shown in Fig. 16.

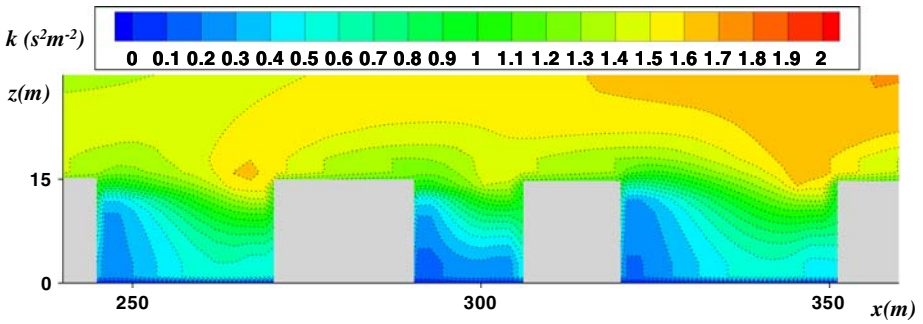

Fig. 17 The turbulent kinetic energy for different aspect ratios $H/W = 0.6$, 1.0, and 0.5 at 1500 local time

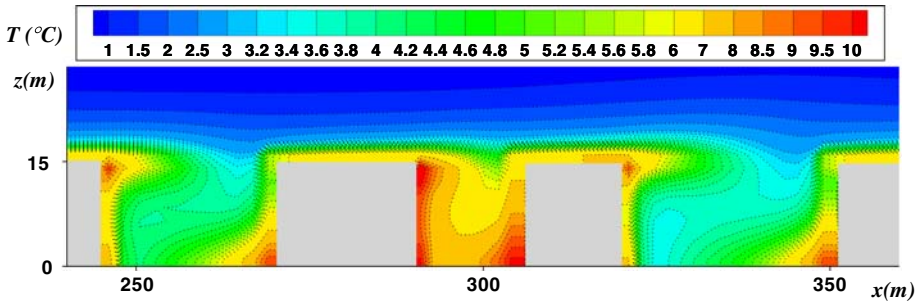

Fig. 18 Temperature difference between the local and reference value for different aspect ratios $H/W = 0.6$, 1.0, and 0.5 at 1500 local time

Figure 17 shows typical patterns of the turbulent kinetic energy with low values within the canyon cavity and a maximum in the impingement regions. Low turbulent kinetic energy is found close to the leeward face of the obstacles, especially within narrow streets with the canyon aspect ratio $H/W = 1$, where calm conditions were predicted near the ground for all street canyon cavities.

The patterns of the temperature differences between local and reference values are dependent on the in-street flow formation. Significant differences in the temperature field can be seen for a regular $H/W = 1$ and the avenue canyons $H/W = 0.5$ and 0.6 (Fig. 18). Heated air accumulates within the cavity in the areas with little turbulent transport and low wind speeds, specifically for $H/W = 1$. A temperature plume is well displayed close to the leeward side of the obstacles, due to the enhanced vertical flow resulting from additional buoyant forcing.

4.4 Section Summary

High-resolution CFD modelling can reproduce detailed structure of the flow field in the urban environment, which is not achievable by the use of the mesoscale model MM5, for example. The important effects of the microscale urban environment cannot be captured in mesoscale meteorological models. The simulations showed a distinctive influence of urban geometry and thermal effects on the flow dynamics in a standard street canyon ($H/W = 1$). Important flow features include a strong vertical motion induced by the drag force at the obstacles and a maximum of the turbulent kinetic energy at a height of approximately two buildings. The temperature within the street canyon increases and a strong vertical gradient is generated

near the top of the buildings, especially at the times of enhanced solar heating. Modelling results produced by mesoscale models can be improved using the output profiles from CFD local-scale simulations, enabling a more realistic representation of local urban effects. The results of microscale numerical simulations of the Lisbon domain using the CHENSI code show significant flow modification due to thermal effects within the street canyons with different aspect ratios. For example, thermal forcing as a consequence of the windward wall heating acts against dynamical forces destroying a conventional single clockwise vortex. A comparison was made between an isothermal case (without building heating) and a thermal case (with building heating) for a typical summer day in Lisbon. A significant change in the flow structure was observed for a background wind perpendicular to the obstacle.

5 Overall Conclusions

The experimental laboratory observations were successfully used to validate the microscale CFD numerical models CHENSI and VADIS. CHENSI performed better in replicating the experimental results because a modified temperature wall function has been implemented. The model can be successfully used in cases when the heat transfer substantially influences the dynamics of the flow. A considerable flow modification caused by solar heating of building walls within the street canyons was found, and showing that microscale CFD models such as CHENSI are helpful in understanding and correctly simulating micrometeorological conditions in urban environment.

Acknowledgements The present work was carried out within the Advanced Tools for Rational Energy Use towards Sustainability project (ATREUS with emphasis on microclimatic issues in urban applications) in the framework of the European Community Marie Curie Research Training Program. The computer support was provided by the Scientific Council of Institut de Développement et de Recherche pour l'Informatique Scientifique (IDRIS), Orsay, France.

References

Bohnenstengel S, Schlunzen KH, Grawe D (2004) Influence of thermal effects on street canyon circulations. Meteorol Z 13:381–386. doi:10.1127/0941-2948/2004/0013-0381

Borrego C, Martins JM, Tome M, Carvalho A, Barros N, Pinto C (2000) Wind tunnel validation of VADIS, a numerical model simulating flow and dispersion around buildings sets. In: Proceedings of EUROTRAC-2 symposium 2000, Springer, Garmisch-Partenkirchen, Germany, CD-ROM

Borrego C, Tchepel O, Costa AM, Amorim JH, Miranda AI (2003) Emission and dispersion modelling of Lisbon air quality at local scale. Atmos Environ 37:5197–5205. doi:10.1016/j.atmosenv.2003.09.004

Borrego C, Tchepel O, Salmim L, Amorim JH, Costa AM, Janko J (2004) Integrated modelling of road traffic emissions: application to Lisbon air quality management. Cybern Syst Int J 35:535–548. doi:10.1080/0196972049051904

Borrego C, Tchepel O, Costa AM, Martins H, Ferreira J (2007) Urban population exposure to particulate air pollution induced by road transport. In: Air pollution modelling and its application XVII. Springer US Ed., pp 267–276

Chen Y, Kim S (1987) Computation of turbulent flows using an extended k-ε turbulence closure model. Report NASA-CR-179204

Dimitrova R, Sini J-F, Richards K, Schatzmann M (2007) CFD investigation of airflow around a simple obstacle with single heating wall. EURASAP Newsl 63:1–35

Huizhi L, Bin L, Fengrong Z, Boyin Z, Jianguo S (2003) A laboratory model for the flow in urban street canyons induced by bottom heating. Adv Atmos Sci 20:554–564. doi:10.1007/BF02915498

Hunter LJ, Johnson GT, Watson ID (1992) An investigation of three-dimensional characteristic of flow regimes within the urban canyon. Atmos Environ 26B:425–432

Jones WP, Launder BE (1972) The prediction of laminarization with a two-equation model of turbulence. Int J Heat Mass Transf 15(2):301–314. doi:10.1016/0017-9310(72)90076-2

Kelly PM, Jones P, Briffa K (1997) Classifying the winds and weather. Chapter 8. In: Hulme M, Barrow EM (eds) The climate of the British isles: present, past and future. Routledge, London, pp 153–172

Ketzel M, Louka P, Sahm P, Guilloteau E, Sini J-F, Moussiopoulos N (2001) Intercomparison of numerical urban dispersion models—part II: street canyon in Hannover, Germany. Water Air Soil Pollut Focus 2:603–613. doi:10.1023/A:1021301316096

Kim J-J, Baik J-J (1999) A numerical study of thermal effects on flow and pollutant dispersion in urban street canyons. J Appl Meteorol 38(9):1249–1260. doi:10.1175/1520-0450(1999)038<1249:ANSOTE>2.0.CO;2

Kim J-J, Baik J-J (2001) Urban street-canyon flows with bottom heating. Atmos Environ 35(20):3395–3404. doi:10.1016/S1352-2310(01)00135-2

Kovar-Panskus A, Louka P, Sini J-F, Savory E, Czech M, Abdelqari A, Mestayer PG, Toy N (2002a) Influence of geometry on the mean flow within urban street canyons—a comparison of wind tunnel experiments and numerical simulations. J Water Air Soil Pollut Focus 2:365–380. doi:10.1023/A:1021308022939

Kovar-Panskus A, Moulinneuf L, Savory E, Abdelquari A, Sini J-F, Rosant J-M, Robins A, Toy N (2002b) A wind tunnel investigation of the influence of solar-induced wall heating on the flow regime within a simulated urban street canyon. J Water Air Soil Pollut Focus 2:555–571. doi:10.1023/A:1021345131117

Launder BE, Spalding DB (1974) The numerical computation of turbulent flows. Comput Methods Appl Mech Eng 3:269–289. doi:10.1016/0045-7825(74)90029-2

Lévi Alvares S (now Anquetin S) (1991) Simulation numérique des écoulements urbains à l'échelle d'une rue à l'aide d'un module k-ε (in French). PhD thesis, Ecole Centrale de Nantes, France

Louka P, Vachon G, Sini J-F, Mestayer PG, Rosant J-M (2001) Thermal effects on the airflow in a street canyon—Nantes '99 experimental results and model simulations. J Water Air Soil Pollut Focus 2:351–364

Martins JM, Borrego C (1998) Describing the dispersion of pollutants near buildings under low wind speed conditions: real scale and numerical results, Envirosoft 98—development and application of computer techniques to environmental studies. WIT, Las Vegas, pp 149–158

Mestayer PG, Sini J-F, Jobert M (1995) Simulation of wall temperature influence on flow and dispersion within street canyons. In: Proceedings of the 3rd international conference on air pollution, vol 1: turbulence and diffusion, Proto Carras, Greece, pp 109–116

Nakamura Y, Oke TR (1988) Wind, temperature and stability conditions in an east-west oriented urban canyon. Atmos Environ 22(12):2691–2700. doi:10.1016/0004-6981(88)90437-4

Oke TR (1988) The urban energy balance. Prog Phys Geogr 12(4):471–508. doi:10.1177/030913338801200401

Oxizidis S, Dudek AV, Papadopoulous AM (2008) A computational method to assess the impact of urban climate on buildings using modeled climatic data. Energy Build 40:215–223. doi:10.1016/j.enbuild.2007.02.018

Richards K, Schatzmann M, Leitl B (2006) Wind tunnel experiments modelling the thermal effects within the vicinity of a single block building with leeward wall heating. J Wind Eng Ind Aerodyn 94(8):621–636. doi:10.1016/j.jweia.2006.02.003

Ruck B (1993) Wind-tunnel measurements of flow field characteristics around a heated model building. J Wind Eng Ind Aerodyn 50(1–3):139–152. doi:10.1016/0167-6105(93)90069-Z

Santamouris M, Papanikolaou N, Koronakis I, Livada I, Assimakopoulos DN (1999) Thermal and airflow characteristics in a deep pedestrian canyon under hot weather conditions. Atmos Environ 33(27):4503–4521. doi:10.1016/S1352-2310(99)00187-9

Sahm P, Louka P, Ketzel M, Guilloteau E, Sini J-F (2002) Intercomparison of numerical urban dispersion models—part I: street canyon and single building configurations. J Water Air Soil Pollut Focus 2:587–601. doi:10.1023/A:1021349232026

Sini J-F, Anquetin S, Mestayer PG (1996) Pollutant dispersion and thermal effects in urban street canyons. Atmos Environ 30(15):2659–2667. doi:10.1016/1352-2310(95)00321-5

Uehara K, Murakami S, Oikawa S, Wakamatsu S (2000) Wind tunnel experiments on how thermal affects flow in and above urban street canyons. Atmos Environ 34(10):1553–1562. doi:10.1016/S1352-2310(99)00410-0

Vardoulakis S, Dimitrova R, Richards K, Hamlyn D, Camilleri G, Sini J-F, Britter R, Borrego C, Schatzmann M, Moussiopoulos N (2006) Numerical model inter-comparison for a single block building within ATREUS. In: Proceedings of the 10th international conference on harmonisation within atmospheric dispersion modelling for regulatory purposes (HARMO10), Crete, Greece, 17–20 Oct 2006, pp 302–306

Xie X, Liu C-H, Leung DYC (2007) Impact of building facades and ground heating on wind flow and pollutant transport in street canyons. Atmos Environ 41(39):9030–9049. doi:10.1016/j.atmosenv.2007.08.027